

Research article

Carbon dots improved the electrochemical reduction performance of Co/AC particle electrodes for humic acid removal: The dominant role of H^{*}

Wenwen Zhang ^{a,b,c}, Yufei Hui ^a, Jiahui Bi ^a, Hongjie Wang ^{a,b,c,*}, Wenyan Liang ^{d,**}

^a Hebei Key Laboratory of Close-to-Nature Restoration Technology of Wetlands, School of Eco-Environment, Hebei University, Baoding, 071002, China

^b Engineering Research Center of Ecological Safety and Conservation in Beijing-Tianjin-Hebei (Xiongan New Area) of MOE, China

^c College of Life Science, Hebei University, Baoding, 071002, China

^d Beijing Key Lab for Source Control Technology of Water Pollution, Engineering Research Center for Water Pollution Source Control and Eco-remediation, Beijing Forestry University, Beijing, 100083, China

ARTICLE INFO

Keywords:

Electrocatalytic reduction
Hydrogen radicals
Humic acid
Carbon dots
Co

ABSTRACT

In the study, a composite particle electrode containing Co was synthesized using activated carbon and carbon dots as precursors (namely Co-CDs/AC) to degrade humic acid (HA) from wastewater. Field emission scanning electron microscopy, X-ray diffraction, and X-ray photoelectron spectroscopy confirmed that carbon dots (CDs) were successfully introduced into the activated carbon loaded with Co (Co/AC). Introduction of CDs promoted dispersion of Co catalyst and the form of Co catalyst was changed from Co⁰ and CoO to Co₄N. Compared to Co/AC, the removal efficiency and mass transfer rate of Co-CDs/AC increased by 3 and 2.5 times, with the values of 95.5% and 5.7×10^{-5} m/s, respectively. Meanwhile, the energy consumption reduced by 3.8 times, being only 1.45 kWh/gCOD. Moreover, Co-CDs/AC possessed the wide range of acid-base application and could effectively remove other organic contaminants. Except for NO₃⁻, the presence of CO₃²⁻, H₂PO₄⁻ and Cl⁻ inhibited the degradation of HA. Free radical experiments revealed that both •OH and H^{*} were involved in Co-CDs/AC system. The H^{*} was the dominant reactive species responsible for HA removal and the contribution rate of H^{*} reached 52.5%. Differ from other advanced oxidation processes, electrochemical reduction replaced electrochemical oxidation as the dominant in HA degradation. Electrochemical measurements implied that Co-CDs/AC possessed the higher oxygen evolution potentials and lower hydrogen evolution potentials, which promoted the production of •OH and H^{*}, thus improving oxidation and reduction of HA. Moreover, Co-CDs/AC had the higher electrochemical double-layer capacitor in acidic and neutral media, which represented larger active surface area, thus enhancing the active site. Based on the results of intermediate products, HA was decomposed to the alkanes with small molecular weight.

1. Introduction

In recent decades, electrochemical technology has attracted growing concern in the degradation of organic pollutants owing to its high removal efficiency, low secondary pollution, mild reaction condition, and simple operation (Gu et al., 2023; Zhang et al., 2021; Zhou et al., 2004a). During the electrochemical reaction process, organic contaminants can be eliminated through three main pathways: (i) direct electron transfer between organic pollutants and the surface of electrode, (ii) indirect redox reactions mediated by reactive species derived from water electrolysis, such as •OH, H^{*}, •O₂⁻, and ¹O₂ (Jiang et al., 2024;

Zhang and Qu, 2024), and (iii) indirect redox processes involving electrochemically generated reactive species from dissolved ions, such as SO₄•⁻, Cl[•], and Cl₂•⁻ (Gao et al., 2020; Lei et al., 2021, 2022; Liu et al., 2024). The degradation and removal of organic pollutants is typically performed in a conventional two-electrode system. However, the system faces limitations stemming from inherent drawbacks, such as insufficient mass transfer, high energy consumption, and low current efficiency (Wang et al., 2022; Zhang et al., 2023; Zhou et al., 2004b).

A three-dimensional electrochemical system consists of an anode, a cathode, and particle electrode bed filled between the gap of two plate electrodes (Li et al., 2023). Under an applied electric field, each particle

* Corresponding author. Hebei Key Laboratory of Close-to-Nature Restoration Technology of Wetlands, School of Eco-Environment, Hebei University, Baoding, 071002, China.

** Corresponding author.

E-mail addresses: wangjh@hbu.edu.cn (H. Wang), lwy@bjfu.edu.cn (W. Liang).

electrode functions as a microelectrode, with one side acting as an anode and the opposite side as a cathode. Therefore, electrochemical reactions occur not only on the surface of plate electrodes but also on all particle electrodes (Yu et al., 2020). Compared with two-electrode system, the incorporation of particle electrodes with higher surface area significantly enhances the availability of active sites. Consequently, the characteristics of particle electrode critically determine the efficiency of three-dimensional electrochemical system. Table S1 presented commonly used particle electrodes, including metal oxides, carbon materials and composites. The outstanding performance of particle electrodes is fundamentally governed by key properties, including high electrical conductivity, substantial surface area, strong adsorption, effective electrocatalytic activity, and long-term stability (Xu et al., 2023). Compared with metal oxides and carbon materials, the composites that are composed of catalysts and their carriers have become promising. Up to now, the three-dimensional electrochemical system has been extensively applied for the degradation of various contaminants, including methylene blue, phenol, landfill leachate, and carbamazepine (Li et al., 2024a,b; Ye et al., 2023).

Co-based catalysts demonstrate significant potential in catalytic application because of their cost-effectiveness and exceptional catalytic performance. Common catalyst supports for Co-based catalysts include metal oxides (e.g., Al_2O_3 , TiO_2 and ZrO_2), zeolites, carbon materials (e.g., activated carbon), and MOF materials (e.g., ZIF-76 and ZIF-8) (He et al., 2025; Huang et al., 2025; Wang et al., 2025). Metallic Co exhibits a facile H adsorption pathway, enabling the generation of abundant adsorbed hydrogen through the activation of H_2O or H^+ under applied cathode potential. The process enhances the reduction degradation of pollutant. Additionally, the presence of Co catalyst facilitates Fenton-like reactions, thereby accelerating the oxidation degradation of pollutants. When there are oxidants (such as persulfate) in the solution, the complexes (e.g. $\text{Co-S}_2\text{O}_8$) can be firstly formed as the main reactants. In addition, ^1O_2 and $\bullet\text{O}_2^-$ can be also produced (Wen et al., 2023). Currently, Co-based catalysts (e.g., CoO , Co_2O_3 , and Co_3O_4) have been extensively utilized in H_2O_2 activation, O_3 -based system, electrocatalysis, photocatalysis, and peroxymonosulfate activation (Ding et al., 2025; Lyu et al., 2025; Zhao et al., 2024). However, the application of metallic Co catalyst as particle electrodes for degrading organic contaminants remains relatively unexplored.

Humic acid (HA) constitutes one of the key components in actual wastewater, including landfill leachate, peat water, and medical wastewater (Jiang et al., 2025; Zhu et al., 2023). Despite HA being a non-toxic substance, its functional moieties (e.g., carboxylic and phenolic hydroxyl groups) are capable of binding with other organic and inorganic substances, thereby forming new pollutants such as trihalomethanes and haloacetic acids (Jing et al., 2023; Mohsin et al., 2021; Satishkumar et al., 2025). HA has posed significant challenges to water treatment process and human well-being owing to its recalcitrant property (Trellu et al., 2016). Therefore, HA was involved as the model for macromolecular and non-biodegradable target substance. Recently, we have prepared a kind of Co-based particle electrode using activated carbon as carrier (namely Co/AC) to degrade HA in three-dimensional electrochemical system (Zhang et al., 2021). Despite the promising results, there were still some problems: (i) agglomeration of Co catalyst in activated carbon carrier, (ii) deterioration performance in alkaline environment or in the presence of NO_3^- . Consequently, the development of new electrode materials is essential to enhance catalytic performance and environmental adaptability.

Carbon dots (CDs), zero-dimensional carbon nanomaterials, are increasingly investigated in electrocatalysis/photocatalysis owing to their nanoscale dimensions (<10 nm), rich and cheap precursor, and unique physicochemical property (Rani et al., 2020). During the electrochemical reaction process, CDs can act as not only electron acceptors by accepting electrons but also electron donors by giving electrons (Chen et al., 2025; Zu et al., 2017). Due to the abundance of covalent and non-covalent functional groups, CDs can not only be used as the sole

catalyst but also couple with metals or metal oxides to form stable composites for electrochemical application (Chen et al., 2025; Lu et al., 2023). However, most research on CDs only focused on the preparation of efficient electrocatalyst/photocatalyst for hydrogen and oxygen evolution reaction (Li et al., 2022; Yang et al., 2019), as well as photocatalytic removal of pollutants. Moreover, study on electrochemical removal of pollutants using CDs has rarely been reported. It was uncertain whether the introduction of CDs would resolve the agglomeration of Co catalyst and eliminate the deterioration performance on the degradation of HA in alkaline environment or in the presence of NO_3^- . Hence, it is essential to clarify the function and mechanism of CDs in degradation of HA.

Therefore, the novel particle electrode that was composed of Co catalyst, powder activated carbon, and carbon dots (namely Co-CDs/AC) was proposed to degrade HA. The physicochemical and electrochemical characterization of Co-CDs/AC were investigated. The effects of CDs, pH values, co-existing anions and other pollutants on the degradation of HA were studied. The dominant reactive species for the degradation of HA were determined and the potential degradation mechanism in Co-CDs/AC system was proposed.

2. Experimental

2.1. Materials

The details of materials were unfolded in Supplementary Materials (Text. S1).

2.2. Preparation and characterization of Co-CDs/AC

Firstly, citric acid (31.52 g) and urea (30.03 g) were dissolved in 100 mL of deionized water at a mass ratio of 1:1 and thoroughly mixed. The mixed solution was placed into a 250 mL polytetrafluoroethylene reactor, sealed and placed in an oven for 8 h at 200 °C. After cooling to room temperature, the above solution was centrifuged (10,000 rpm, 20 min) to remove suspended matter. The supernatant was dialyzed (500–1000 Da, 48 h) to purify CDs. Secondly, the Co-CDs/AC electrodes were prepared by impregnation calcination method. 35 g powder activated carbon was impregnated in 250 mL CDs solution (15 mg/L). The mixed solution with 0.1 mol/L $\text{Co}(\text{NO}_3)_2$ addition was stirred at 25 °C for 8 h, and then dried at 105 °C. The obtained powder was mixed with self-made polyvinyl alcohol adhesive to form particles (Zhang et al., 2021). The CDs-doped Co loaded activated carbon particle electrode was obtained by calcination at 600 °C for 4 h in nitrogen, namely Co-CDs/AC. Co/AC particle electrode was prepared by a similar method to use as comparison. The different methods of Co-CDs/AC characterization were summarized in the Text S2 and Text S3.

2.3. HA degradation experiments

The electrocatalytic experiment was performed using the same reactor as our previous reports (Zhang et al., 2021). A total of 15 g Co-CDs/AC particle electrodes were placed in the reactor with an effective volume of 60 cm³. Before electrocatalytic experiments, the Co-CDs/AC electrodes were adsorbed and saturated. The electrocatalytic experiment of HA (200 mg/L, 540 mL) was performed at 3.34 mA/cm² and hydraulic retention time (HRT) of 10 min. 0.01 M Na_2SO_4 served as the electrolyte and the initial pH of solution was adjusted 7.0 by adding 0.1 M H_2SO_4 and 0.1 M NaOH as required. The treated HA samples were discharged directly without circulation. Samples were systematically collected from the outlet every 20 min for chemical oxygen demand (COD) determination by COD rapid tester (CTL-12, Chengde Huatong Environmental Protection Co., Ltd).

Electrocatalytic experiments with or without circulation (Fig. S1) were performed using Co-CDs/AC and Co/AC electrodes to determine the role of CDs on HA degradation. In addition, the effects of pH (5.0,

7.0, 9.0 and 11.0), coexisting anions (PO_4^{3-} , CO_3^{2-} , NO_3^- , and Cl^-), and pollutants (methyl orange (MO), tetracycline hydrochloride (TCH), and phenol (PhOH)) on HA degradation were carried out. Five cyclic experiments were conducted to verify the stability of Co-CDs/AC.

The mass transfer coefficient (k_m) in Co-CDs/AC system was obtained according to Comninellis' method (Eqs. (1)–(3)) (Fan et al., 2019).

$$I_{lim} = n F k_m C \quad (1)$$

$$I = \alpha I_{lim}^0 \quad (2)$$

$$\ln C(t) = \frac{A k_m}{V_E} t + \ln(\alpha C_0) + \frac{1 - \alpha}{\alpha} \quad (3)$$

Where I_{lim} represents the limiting current density (mA/cm^2), n denotes the number of electrons, F is the Faraday constant, A signifies the anode area (m^2), V_E stands for the electrolyte volume (m^3), and α represents the characteristic electrolysis parameter.

2.4. Identification of active species

ESR determination. 50 mmol/L DMPO was used as the trapping agent. After 1, 2 and 4 min of electrolysis, 1 mL sample was collected from self-made three-dimensional electrochemical system. The spectra were acquired using an X-band ESR spectrometer (EMX Plus, Bruker, Germany) at ambient temperature (298 K). The measurements were performed with a central magnetic field of 3510 G, a sweep width of 100 G, and a microwave frequency of 9.77 GHz.

Quenching experiments. TBA was used as a quenching agent. A series of TBA concentrations (50, 100 and 200 mM) were incorporated into the HA solution.

Competitive kinetic experiment of free radicals and determination of second-order rate constant. The pCBA (10 mg/L) and different concentrations of TBA (50, 100 and 200 mmol/L) were simultaneously incorporated into the HA solution. The concentration of $\cdot\text{OH}$ was quantified based on Eq. (4).

$$\int_{t=0}^t [\cdot\text{OH}] dt = \frac{1}{k_{\cdot\text{OH}/pCBA}} \ln \left(\frac{[pCBA]_0}{[pCBA]_t} \right) \quad (4)$$

where $t = 0$ and t represent the initial and time-dependent concentrations of pCBA (mol/L), respectively, $[\cdot\text{OH}]$ denotes the hydroxyl radical concentration (mol/L), and $k_{\cdot\text{OH}/pCBA}$ quantifies the second-order reaction kinetics between $\cdot\text{OH}$ and pCBA.

2.5. Analytical methods

The concentration of total organic carbon (TOC) after filtration (0.45 μm) by TOC analyzer (TOC-VCSN, Shimadzu, Japan). The analytical methods of intermediate products by UV-vis spectrum, 3DEEM fluorescence spectroscopy and GC-MS were listed in the Text S4. The absorbance of 400 nm was determined by UV-vis spectrophotometer. The concentration of pCBA was determined by high-performance liquid chromatography (HPLC, 1260, Agilent, USA) equipped with a C18 column (Agilent TC-C18, 4.6 \times 250 mm, 5 μm) at 1 mL/min. A 45:55 (v:v) mixture of H_3PO_4 (10 mmol/L) and methanol served as the mobile phase. Energy consumption (EC) and current efficiency (CE) were determined using Eqs. (5) and (6), respectively.

$$EC = \frac{U I t / V}{\Delta COD} \times 1000 \quad (5)$$

$$CE(\%) = \frac{(COD_0 - COD_t) F V}{8 I t} \quad (6)$$

Where I denotes the applied current (A), U represents the applied

voltage (V), t signifies the electrolysis time (h), ΔCOD indicates the reduction amounts of COD during electrocatalysis (mg/L), V is the volume of HA solution (L), and F corresponds to the Faraday constant (96,485 C/mol).

2.6. Statistical analysis

TriPLICATE experiments were performed and data were analyzed using one-way analysis of variance (ANOVA) (SPSS 20.0, USA). Significance wet set at $p < 0.05$ unless noted.

3. Results and discussion

3.1. Characterization of Co-CDs/AC

The synthesized CDs exhibited blue fluorescence, with their maximum absorption peak at 330 nm and fluorescence excitation/emission peaks at 338 and 435 nm, respectively (Fig. S2). TEM images (Fig. S3) revealed that the CDs were monodispersed spherical particles with an average diameter of 1.81 nm and a lattice spacing of 0.207 nm, which was assigned to the (100) plane of graphite (Zhou et al., 2015). The diffraction peak at 27.5° in Fig. S4 was belonged to the (110) crystal plane of sp^3 -hybridized carbon nitride (Hao et al., 2024), while a minor peak at 43.2° aligned with the (100) graphene plane, exhibiting a lattice fringe distance of 0.207 nm (Guo et al., 2022), which was consistent with the TEM observation. XPS analysis (Fig. S5) confirmed the presence of carbon (C), nitrogen (N), and oxygen (O) in the CDs. The C1s spectrum displayed three peaks at 284.7 (C-C=C), 285.4 (C-O/C-N), and 288.3 eV (C=O) (Wang et al., 2025). In the N1s spectrum, peaks at 399.7 eV and 401.4 eV were attributed to pyrrolic N and graphitic N, respectively (Lu et al., 2023). The O1s spectrum showed two peaks at 531.5 (C-O) and 532.9 eV (C=O) (Wang et al., 2025). These findings collectively demonstrated the successful synthesis of the CDs.

Fig. S6 displayed the surface morphology of Co-CDs/AC. After only loading Co catalyst, there were large crystals and pores on the surface of activated carbon (Zhang et al., 2021). The introduction of CDs led to the disappearance of pores and large crystals (Fig. S6a–6d), which was beneficial to the dispersion of Co catalyst in activated carbon carrier. Meanwhile, Co was found to be evenly dispersed in Co-CDs/AC, as confirmed by Co mapping. In addition to C, O, and Co elements, N was also observed (Fig. S6e–6h). This was attributed to the use of urea as a raw material in the synthesis of CDs, which supplied a rich N source. As shown in Fig. 1a, the two broad peaks at 20–30° and 40–50° confirmed the amorphous structure of activated carbon. The peaks at 44.3°, 52.3°, and 77.2° were observed, which were assigned to the (111), (200), and (220) crystal planes of face-centered cubic Co_4N (JCPDS 41-0943) (Li et al., 2025). Different from Co/AC (Zhang et al., 2021), the crystal phase of Co catalyst changed from Co^0 and CoO to Co_4N . The result showed that the introduction of CDs could change the crystal phase composition of Co catalyst. Therefore, Co was not oxidized owing to the ligand protection of CDs, and it might cooperate with N to form the Co-N bond.

The XPS full spectrum showed the existence of C, O, N, and Co elements (Fig. S7), which was consistent with the result of element mapping detection. In the Co 2p spectrum (Fig. 1b), the peaks at 783.3 (Co 2p_{3/2}) and 798.7 eV (Co 2p_{1/2}) were observed (Li et al., 2025). For Co 2p_{3/2} spectrum, three peaks at 777.6, 780.1 and 783.1 eV were attributed to Co-Co, Co-O and Co-N bonds, respectively (Zhang et al., 2023). The Co 2p_{1/2} peak at 798.5 eV further confirmed the presence of Co-N bond, supporting the formation of Co_4N (Yang et al., 2019). In the O 1s spectrum (Fig. 1c), the peaks at 528.8, 530.4 and 531.1 eV were assigned to lattice oxygen in the Co-O bond, oxygen of hydroxide ions and physically adsorbed H_2O , respectively (Wu et al., 2025). For N 1s spectrum (Fig. 1d), three peaks at 395.7, 398.90, and 401.60 eV were ascribed to pyrrole N, pyridine N, and graphite N (Liang et al., 2024; Wu et al., 2024), with the relative content of 33.8 %, 56.7 %, and 9.5 %,

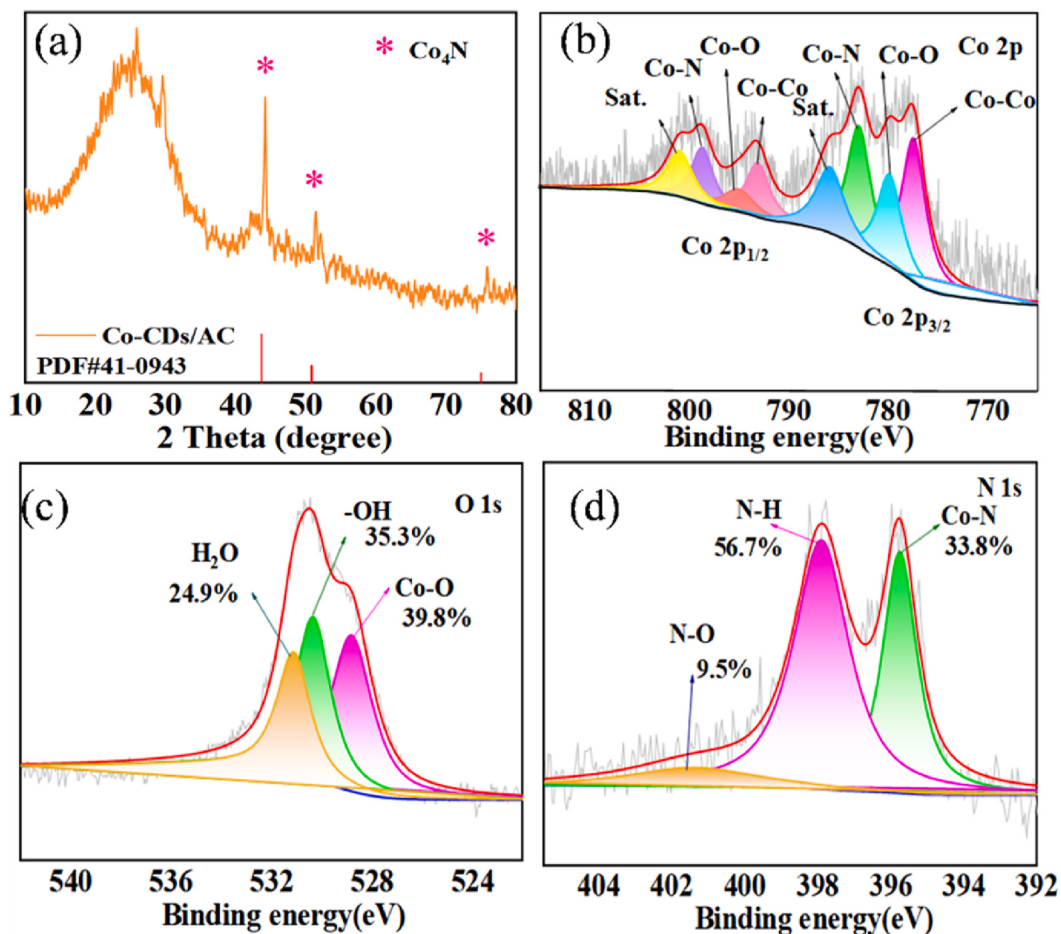


Fig. 1. XRD pattern (a) and XPS spectra of Co-CDs/AC. Co 2p spectrum (b), O 1s spectrum (c), and N 1s spectrum (d).

respectively. Among them, pyridine N was regarded as the main active site in the catalytic reaction, promoting electron transfer (Zhang et al., 2020). Therefore, the presence of pyridine N in the Co-CDs/AC electrode could increase electron density and mobility in the π conjugated frame of N, accelerating the degradation of pollutants (Li et al., 2025).

3.2. Degradation performance of Co-CDs/AC

3.2.1. The role of CDs

In order to study the role of CDs on the degradation and removal of HA, control experiments were performed at 3.34 mA/cm² and HRT of 10 min. The removal efficiency of Co-CDs/AC reached 95.5 %, which

was 3 times that of Co/AC (Fig. 2a). Introduction of CDs obviously improved the electrocatalytic degradation capability of the Co/AC electrode. This was because the active sites increased by regulating electron redistribution (Ge et al., 2020). Due to rich functional groups with covalent and non-covalent bonds, CDs can be coupled with Co to form Co₄N, promoting the degradation of HA.

In addition, compared with Co/AC (5.44 kWh/gCOD), the energy consumption of Co-CDs/AC decreased to 1.42 kWh/gCOD (Fig. 2a). The incorporation of CDs led to a noticeable reduction in the energy consumption of Co/AC system. Compared with the electrode materials from other studies (Table S1), Co-CDs/AC exhibited superior performance in HA degradation. The current density was only 3.34 mA/cm², which was

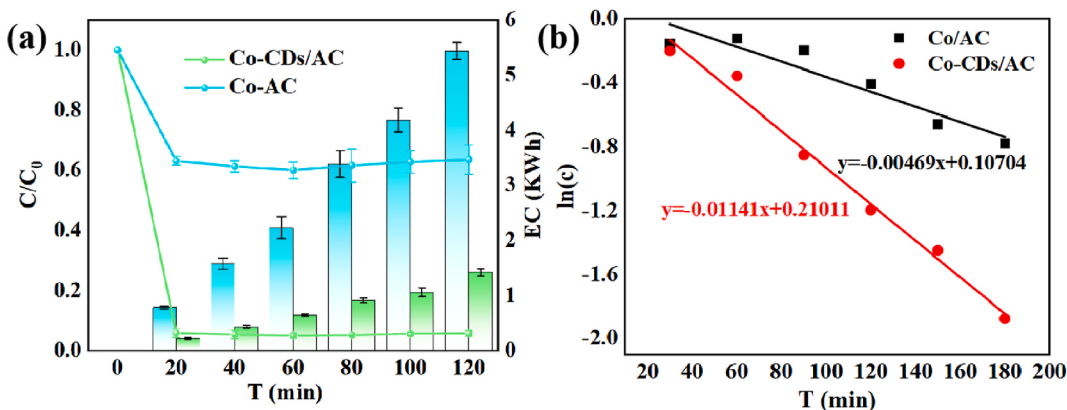


Fig. 2. The effect of CDs on the degradation of HA. (a) Removal efficiency and energy consumption. (b) Linear fitting of degradation kinetics of HA.

lower than 5.68 and 6.0 mA/cm² in other studies (Capasso et al., 2019; Yin et al., 2020). Co-CDs/AC achieved over 90 % HA removal in just 20 min, whereas prior studies required more than 60 min (Du et al., 2022; Liu et al., 2019a; Sarno et al., 2019). Moreover, the HA initial concentration used (200 mg/L) was significantly higher than those reported (5–50 mg/L) (Bazrafshan et al., 2012; Dargahi et al., 2022; Tang et al., 2014).

Fig. 2b showed the fitting curve of degradation kinetics of Co/AC and Co-CDs/AC. The average mass transfer coefficient could be determined by the slope of the relevant line. The k_m value of Co-CDs/AC was 5.7×10^{-5} m/s, which was 2.5 times that of Co/AC. This result meant that introduction of CDs enhanced the mass transfer rate of Co/AC. Compared with other electrochemical reactors (Table 1), the k_m value of Co-CDs/AC was higher, which further suggested faster mass transfer and better electrocatalytic performance.

3.2.2. Environmental application

Co-CDs/AC presented excellent degradation performance across a broad pH range (5.0–11.0) (Fig. 3a), demonstrating its versatility in both acidic and alkaline conditions. Differ from our previous study, the removal efficiency of HA dropped to 59.7% and 78.1% at 9.0 and 11.0, respectively (Zhang et al., 2021). These findings suggested that introduction of CDs could eliminate the deterioration performance of Co/AC on HA degradation in alkaline environment. This might be because the presence of Co-N enabled Co-CDs/AC stable in harsh acidic or basic conditions (Qin et al., 2021).

CO_3^{2-} and H_2PO_4^- severely hindered HA degradation (Fig. 3b). When CO_3^{2-} was added, the removal efficiency of HA decreased from 95.5% to 42.4%. CO_3^{2-} could react with $\bullet\text{OH}$ to produce OH^- and $\text{CO}_3\bullet$ (Xu et al., 2019). The produced $\text{CO}_3\bullet$ exhibited limited oxidative capacity, rendering it ineffective for oxidizing most organic pollutants. Moreover, the hydroxide ion generated from hydrolysis of CO_3^{2-} could react with $\bullet\text{OH}$ to produce peroxy radical (Wang and Wang, 2021). After the addition of H_2PO_4^- , the HA removal decreased to 35.8%. This was due to the fact that H_2PO_4^- in the solution could react with $\bullet\text{OH}$ to produce OH^- and $\text{HPO}_4\bullet$ (Wang et al., 2019). The presence of Cl^- inhibited HA degradation and the removal reduced to 79.9%. Cl^- reacted with $\bullet\text{OH}$, generating reactive chlorine species, such as $\bullet\text{Cl}$, $\bullet\text{Cl}_2^-$, $\bullet\text{ClO}$, $\bullet\text{ClO}_2^-$, and Cl_2 (Li et al., 2023). NO_3^- had no significant effect on the degradation of HA ($p > 0.05$). Differ from our previous studies, the addition of NO_3^- reduced HA removal to 25.1 % (Zhang et al., 2021). Introduction of CDs eliminated the inhibition effect of Co/AC on HA degradation in the presence of NO_3^- . Since NO_3^- could react with H^* radicals, yielding NO_2^- , N_2 , NH_4^+ , and other redox products (Xu et al., 2018).

Some other contaminants (such as MO, TCH, and PhOH) were used to evaluate the application potential of Co-CDs/AC electrodes. As depicted in Fig. 3c, the removal efficiencies of HA, MO, TCH, and PhOH were 95.5%, 97.5%, 98.3% and 91.1%, respectively. These findings suggested that the Co-CDs/AC electrode displayed remarkable versatility in degrading diverse organic contaminants in aqueous solutions.

Table 1
Comparison of k_m for pollutant degradation among various electrochemical reactors.

Anode structure	Reactor type	k_m (m/s)	Reference
Square plate anode	Separation reactors	3.9×10^{-6}	Lizhang et al. (2016)
Reticulated anode	Vertical flow tubular reactor	7.8×10^{-6}	Wang et al. (2015)
Reticulated anode	Rotating multi-electrode electrochemical reactor	1.6×10^{-5}	Fan et al. (2019)
Reticulated anode	Co/AC particle electrode bed reactor	2.3×10^{-5}	This study
Reticulated anode	Co-CDs/AC particle electrode bed reactor	5.7×10^{-5}	This study

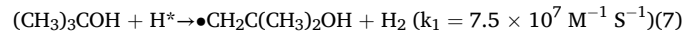
To evaluate the catalytic stability of Co-CDs/AC, cyclic experiments were conducted in the Co-CDs/AC system. Additionally, the removal efficiency of HA only decreased by 5.4% after 5 cycles (Fig. 3d). These results indicated that the Co-CDs/AC particle electrode demonstrated good stability and electrocatalytic performance.

3.3. Degradation mechanism of Co-CDs/AC

3.3.1. Identification of free radical

As illustrated in Fig. 4a, the peaks of DMPO-OH (1:2:2:1, $a_N = a_H = 1.45$ mM) and DMPO-H (1:1:2:1:2:1:1, $a_N = 1.55$ G, $a_H = 2.06$ G) adducts were detected, confirming the participation of $\bullet\text{OH}$ and H^* radicals in Co-CDs/AC system. Compared with Co/AC system, the $\bullet\text{OH}$ signal at 1 min was more obvious in Co-CDs/AC system, suggesting that there were more $\bullet\text{OH}$ radicals generated from the reduction of H_2O (Lee et al., 2024). After 2 min of electrolysis, the intensity of $\bullet\text{OH}$ signal in Co/AC system became strong, while the $\bullet\text{OH}$ signal was changed to H^* in Co-CDs/AC system. The result meant that introduction of CDs promoted the production of H^* radical and made H^* be the dominant radical in Co-CDs/AC system. Moreover, the intensity of H^* signal in Co-CDs/AC was still obvious after 4 min of electrolysis. Differ from Co/AC system, reduction replaced oxidation as the dominant reaction in Co-CDs/AC system. At a certain cathodic potential, the presence of Co-Co could accelerate the reduction of H_2O to generate H^* (Zhang et al., 2018). The formation of Co_4N enabled Co-CDs/AC could promote the production of H^* under an applied electric field (Gudimella et al., 2022). It explained the reason why the degradation of HA was not affected with addition of NO_3^- in Co-CDs/AC system.

Fig. 4b-d displayed the results of quenching experiments. When TBA reached 50 mM, the degradation of HA in Co/AC system showed a strong inhibition of 80.7%, while the inhibition in Co-CDs/AC system was only 31.5%. This result implied that $\bullet\text{OH}$ was crucial for HA degradation in Co/AC system. As the concentration of TBA rose to 100 mM, there was no significant difference on the inhibition in Co/AC system ($p > 0.05$). Therefore, the contribution rate of $\bullet\text{OH}$ could reach 80.7% in Co/AC system. However, after the addition of 100 mM TBA in Co-CDs/AC system, the inhibition quickly rose to 73.1%, and then further increased to 84.0% at 200 mM. Differ from Co/AC system, the contribution rate of $\bullet\text{OH}$ was only 31.5% and there was other free radical that contributed to 52.5% in Co-CDs/AC system. Some studies have suggested that TBA could be used as the H^* radicals quenching reagent and higher concentration of TBA could quench more H^* radicals (Feng et al., 2025; Lymar et al., 2012; Wang et al., 2022). H^* radicals could react with TBA to generate c-center 2-hydroxy-2-methylpropyl radical according to Eq. (7) (Lymar et al., 2012). At the same time, TBA could convert hydrogen radicals into relatively inert 2-methyl-2 propanol radicals (Liu et al., 2019b; Mezyk et al., 2004). Therefore, H^* radical was the dominant in Co-CDs/AC system and the contribution rate of H^* radical was 52.5%. It was consistent with the results of ESR.



*p*CBA has been widely employed as a probe to quantify $\bullet\text{OH}$. The $\bullet\text{OH}$ level was assessed by analyzing the competitive kinetics of *p*CBA and HA. As depicted in Fig. 4e, compared with Co/AC system (2.5×10^{-10} M s), the production amount of $\bullet\text{OH}$ in Co-CDs/AC system was lower, with being 1.7×10^{-10} M s. Moreover, the second order rate constant $k_{\bullet\text{OH}/\text{HA}}$ in Co-CDs/AC system was calculated to be $8.5 \times 10^9 \text{ L/mol}\cdot\text{s}$, which was slightly lower than that of Co/AC system ($11.9 \times 10^9 \text{ L/mol}\cdot\text{s}$) (Fig. S8). These results further suggested that the introduction of CDs decreased the electrochemical oxidation degradation of HA.

Combining the results of ESR, TBA and *p*CBA, the H^* replaced $\bullet\text{OH}$ radical being a dominant reactive species generated in Co-CDs/AC system. Therefore, it was believed that electrochemical reduction rather than electrochemical oxidation that played a dominant role in Co-CDs/AC system. Different from other advanced oxidation processes, where

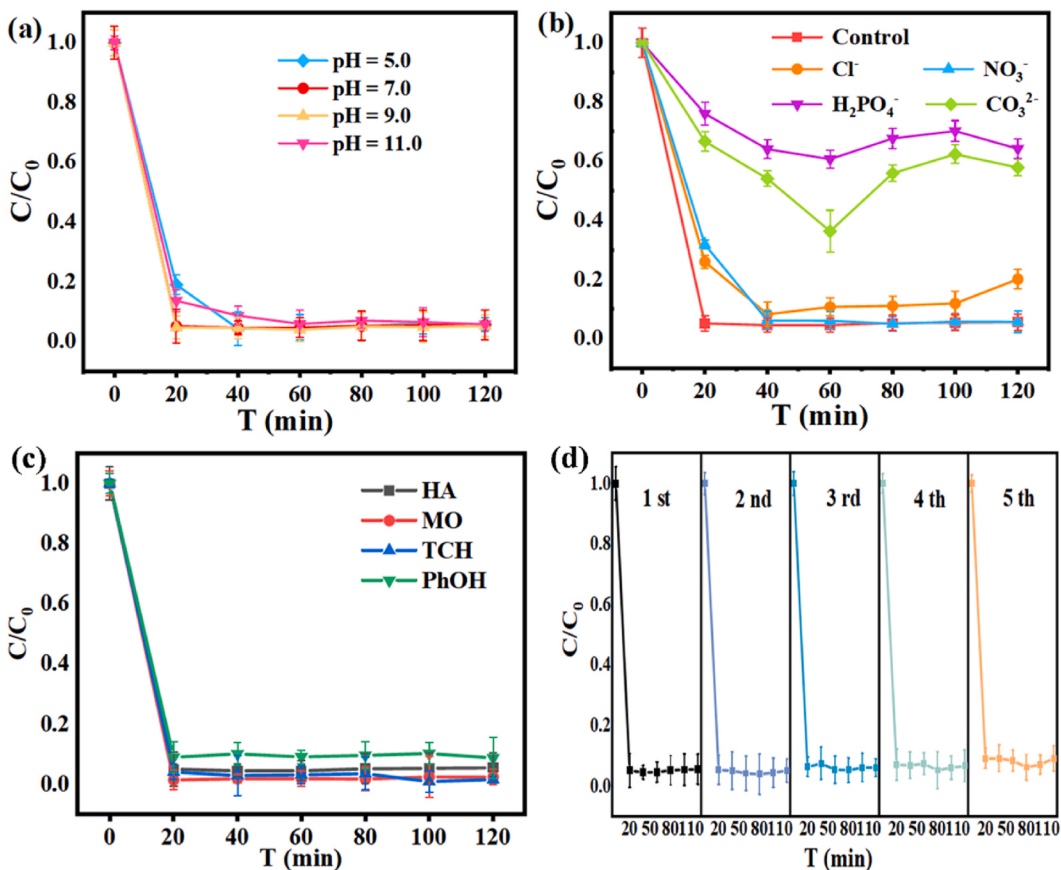


Fig. 3. Effects of pH values (a) and inorganic anions (b) on the degradation of HA in Co-CDs/AC system. Removal efficiencies of different contaminants (c) and cycling runs in the electrocatalytic degradation of HA (d).

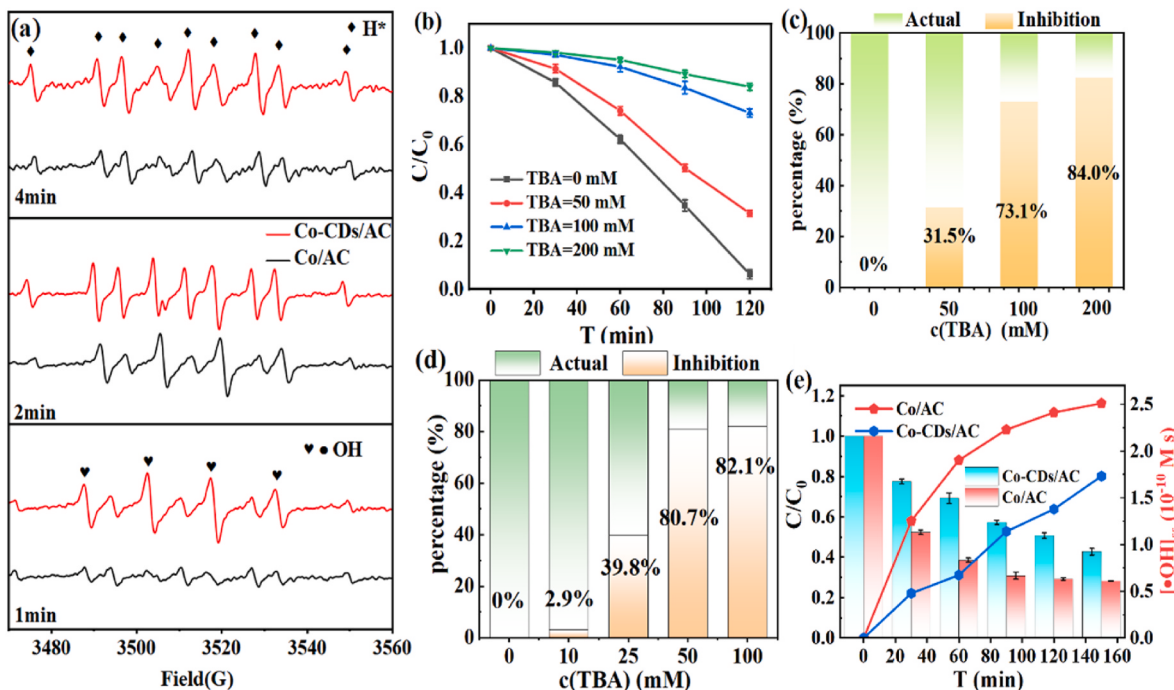


Fig. 4. The ESR spectra after electrolysis in Co-CDs/AC and Co/AC system (a). The effect of TBA on the degradation of HA in Co-CDs/AC (b–c) and Co/AC (d) system. (e) The production of $\bullet\text{OH}$ assessed with pCBA in Co-CDs/AC and Co/AC system.

the HA was degraded by the oxidation. In the present study, the electrochemical reduction replaced electrochemical oxidation as the dominant reaction in the Co-CDs/AC system.

3.3.2. Electrocatalytic performance of Co-CDs/AC

The hydrogen evolution potential (HEP) and oxygen evolution potential (OEP) played critical roles in determining the electrochemical performance of electrode materials. The results of linear sweep voltammetry showed the OEP of Co-CDs/AC were 2.13, 2.25, and 1.52 V (vs. RHE) in acidic, neutral, and alkali media, respectively (Fig. S9a), which were higher than that of Co/AC (1.67, 1.95, and 1.59 V (vs. RHE)) (Zhang et al., 2021). The introduction of CDs resulted in an elevated OEP of Co/AC in acidic and neutral media, which mitigated undesired oxygen evolution side reactions and enhanced the electrochemical oxidation of HA. Moreover, the corresponding Tafel slopes of Co-CDs/AC were 199, 371 and 51 mV/dec, respectively, in acidic, neutral and alkaline media (Fig. S9b). As presented in Fig. S9c, compared with Co/AC (0.37 and 0.77 V (vs. RHE)) in acidic and neutral media (Zhang et al., 2021), the HEP of Co-CDs/AC decreased to 0.25 and 0.34 V (vs. RHE), respectively. The lower HEP meant that more H^* could be generated. The addition of CDs promoted the production of H^* radicals, thus accelerating the electrochemical reduction degradation of HA. Meanwhile, the HEP in alkaline media increased slightly to 0.44 V (vs. RHE). Fig. S9d showed the corresponding Tafel slope of Co-CDs/AC, with being 116, 72, and 94 mV/dec, respectively, in acidic, neutral, and alkaline media.

Cyclic voltammetry (CV) at various scan rates in the non-Faraday potential region is commonly used to obtain the electrochemically active surface area (ECSA), which represents the density of electroactive sites on the catalyst (Fig. S9e–g)). Compared with Co/AC, the

electrochemical double-layer capacitors (C_{dl}) of Co-CDs/AC in acid and neutral media increased from 9.18 to 0.68 mF/cm² to 15.26 and 0.89 mF/cm², respectively. The introduction of CDs expanded the active surface area of Co/AC, enhancing the exposure of active sites.

The CV results (Fig. 5a) revealed distinct oxidation and reduction peak at 0.92 V and 0.61 V (vs. RHE), which were assigned to the transitions of $Co^{2+} \rightarrow Co^{3+}$ and $Co^{3+} \rightarrow Co^{2+}$, respectively (Huang et al., 2022; Veerasubramani et al., 2014). After the addition of 200 mg/L HA, the overall current response was enhanced. The current density of oxidation peak and reduction peak increased from 2.42 to 2.97 mA/cm² and 1.95–2.18 mA/cm², respectively. The results showed that the Co-CDs/AC electrode facilitated the direct oxidation and reduction of HA. The current intensity of oxidation peak was linearly fitted to 1/2 power of scanning speed. The linear equation was I (mA) = $1.602v^{1/2}-0.229$, $R^2 = 0.992$ (inset Fig. 5b). The strong correlation observed in the fitting analysis showed that irreversible adsorption of HA on Co-CDs/AC. Based on the Laviron correlation (Eq. (8)), the electron transfer coefficient ($\alpha = 0.3$) and electron transfer number ($n = 1$) were derived from the slope of E_p vs. $\log v$. This indicated that the oxidation/reduction of HA on Co-CDs/AC was a one-electron transfer process.

$$E_p = -\frac{RT}{anF} \log \left(\frac{anF}{RTK_s} \right) - \frac{RT}{anF} \log v \quad (8)$$

where E_p denotes peak potential (V); v represents scan rate (V/s); F is Faraday constant (96,500 C/mol); K_s stands for diffusion coefficient; R is gas constant (8.314 J/mol K); and T refers to temperature (K).

In the electrochemical impedance spectroscopy (EIS) spectra, the high-frequency semicircular reflects charge-transfer resistance, while the low-frequency linear portion indicates diffusion-controlled behavior

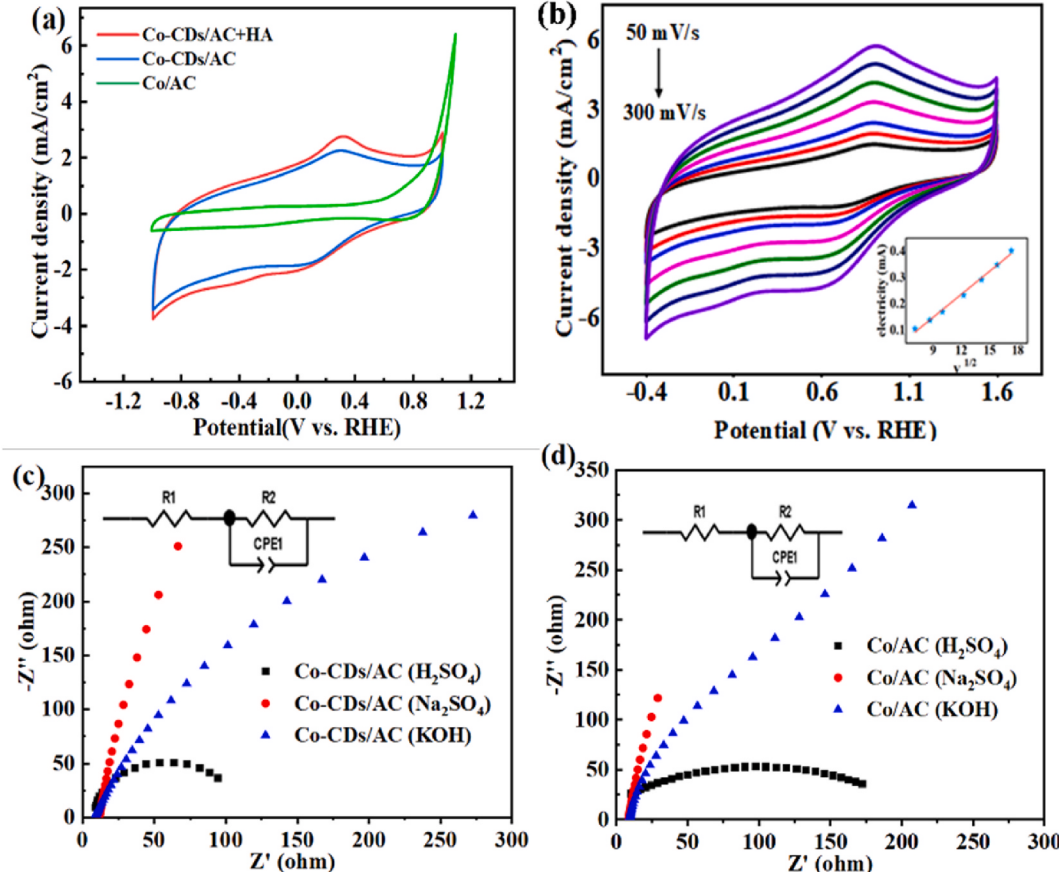


Fig. 5. The CV curves of Co-CDs/AC with 200 mg/L HA were recorded at 50 mV/s (a) and across scan rates from 15 to 300 mV/s (b) in 0.1 mol/L Na_2SO_4 . Fig. 5b displayed the relationship between peak potentials and the logarithm of scan rates. Nyquist curves and equivalent circuits of Co-CDs/AC (c) and Co/AC (d).

(Yang et al., 2019). Regardless of pH (acidic, neutral or alkaline), both Co/AC and Co-CDs/AC exhibited a low-frequency linear region in EIS spectra (Fig. 5c–d), confirming diffusion-controlled behavior with Warburg impedance. Moreover, the center of capacitance reactance deviated from the real axis suggested a dispersion effect. Notably, Co-CDs/AC showed lower resistance (56Ω) in acidic media, enhancing charge transfer efficiency. The constant phase element (CPE) analysis revealed near-ideal capacitive behavior ($CPE-P \approx 1$) for Co-CDs/AC across all pH conditions.

3.3.3. Degradation products

As illustrated in Fig. 6a, spectroscopic analysis of the effluent over time was compared with the raw HA solution. The raw HA exhibited an absorption peak at 240–290 nm, which was attributed to the $\pi-\pi$ transitions in aromatic structures, such as polycyclic aromatic hydrocarbons, olefins, phenols, and benzoic acid (Fukushima et al., 2001). After the electrolysis, the peak vanished, accompanied by a significant absorbance decrease, confirming efficient degradation of unsaturated moieties in HA. Notably, the overall spectral shape remained unchanged, indicating no alteration in product composition.

Due to cost-effectiveness, high selectivity, and sensitivity, 3DEEM spectroscopy has become a preferred method for HA analysis (Mielnik and Kowalcuk, 2018; Valencia et al., 2013). Fig. 6b illustrated that the raw HA solution displayed a fluorescence peak at wavelength/emission wavelength (E_X/E_m) of 460/450 nm, characteristic of humic acid-like compounds (Chen et al., 2003; Sierra et al., 2005). After 20 min of electrolysis (Fig. 6c), the strength of fluorescence peak weakened obviously, indicating that the humic acids-like compounds were degraded in Co-CDs/AC system. When the electrolysis time was over 40 min (Fig. 6d–f), a new fluorescence peak at E_X/E_m of 275/430 nm was attributed to fulvic acid-like compounds. Moreover, the intensity of the

fluorescence peak increased, suggesting that the amount of fulvic acid-like organic was gradually accumulated. The weight-averaged molecular masses of fulvic acid-like compounds (~1 kDa) are approximately 80 % lower than those of humic acids-like compounds (~6 kDa) (Zhang et al., 2018), indicating the fragmentation of large aromatic macromolecules into smaller organic species during the treatment.

GC-MS analysis was performed to identify intermediate products formed during the degradation of HA in Co-CDs/AC system (Table S3). Among the 19 kinds of intermediate products, 94.7 % alkanes were observed, including short-chain alkanes (such as P1, P2, P3, P7–P10, and P12–P15), long-chain alkanes (such as P19), cycloalkanes (such as P4 and P5), along with olefins (such as P11, P16 and P17). Meanwhile, one chemical including N element (P18) was to be found. Conventional biological processes showed limited efficacy against long-chain alkanes ($C_{15}-C_{40}$ alkanes). However, the Co-CDs/AC system achieved significantly mineralization of HA, with concentrations of TOC decreasing from 90.3 mg/L to 5.8 mg/L after 20 min of electrolysis (Fig. S10). These findings confirmed the capacity of Co-CDs/AC system to improve wastewater biodegradability.

3.3.4. Degradation mechanism

The proposed degradation mechanism of HA in Co-CDs/AC system was displayed in Fig. 7. The reaction mechanism included electrochemical oxidation and electrochemical reduction. The catalytic activity of Co-CDs/AC system stems from the unique properties of Co_4N : (i) low hydrogen evolution potential in acidic/neutral conditions; (ii) reversible Co^{2+}/Co^{3+} redox cycling that sustains electron transfer; and (iii) formation of micro-bipolar electrodes under applied potential. Cathodic Co_4N facilitated the reduction of HA via H^* radicals, while anodic Co_4N mediated the oxidation of HA though $\bullet OH$ radicals. Therefore, direct redox of electron transfer, electrochemical oxidation of $\bullet OH$ radical and

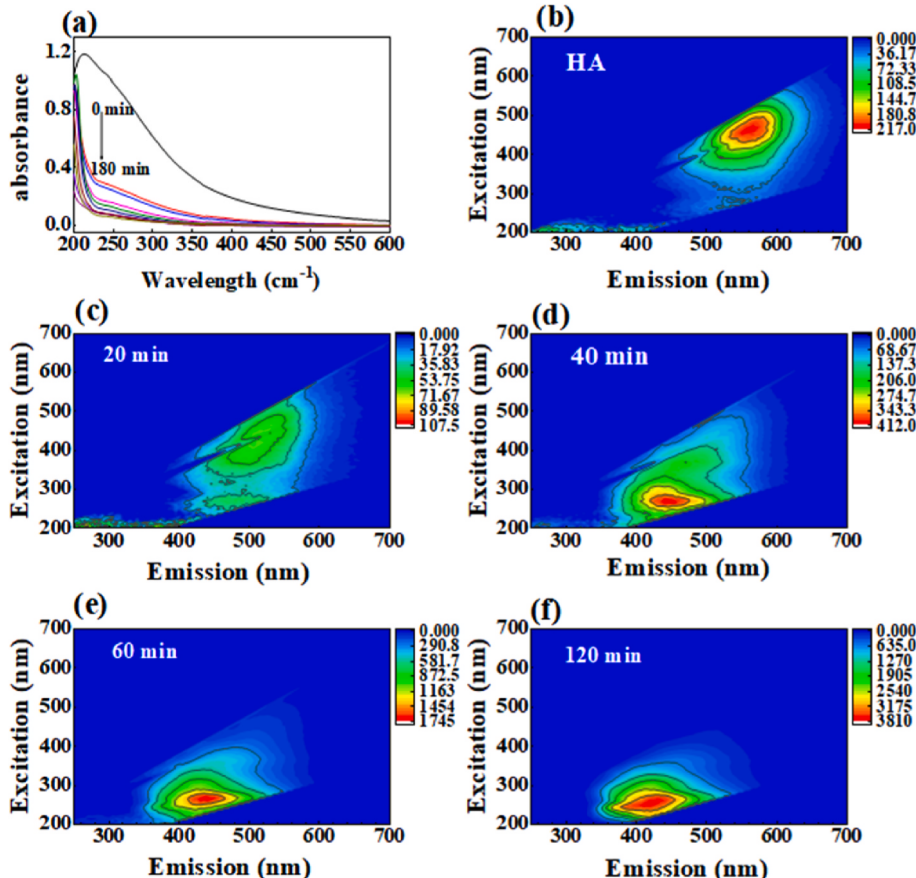


Fig. 6. UV-vis absorption spectra of HA at varying electrolysis times (a). 3D-EEM spectroscopy after 0 (b), 20 (c), 40 (d), 60 (e), and 120 min (f) of electrolysis.

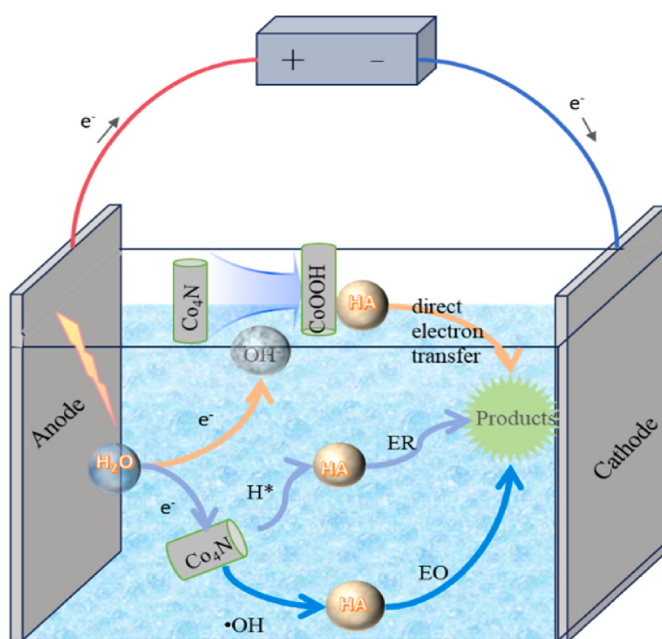
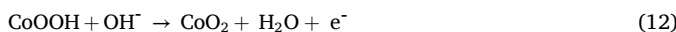
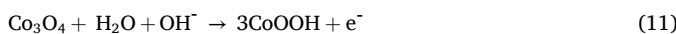
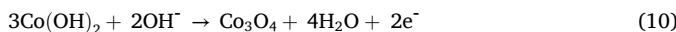


Fig. 7. Degradation mechanism of HA in Co-CDs/AC system.

electrochemical reduction of H^* radical contributed the degradation of HA in Co-CDs/AC system.



4. Conclusions

The prepared Co-CDs/AC particle electrode could achieve excellent electrocatalytic degradation of HA. Introduction of CDs promoted the dispersion of Co catalyst in the activated carbon carrier and the form of Co catalyst was changed from Co^0 and CoO to Co_4N . The Co-CDs/AC system achieved 95.5% removal under current density of 3.34 mA/cm², pH of 7.0, initial HA of 200 mg/L, electrolyte of 0.01 M Na_2SO_4 , and 10 min of HRT. Compared with Co/AC, Co-CDs/AC had a higher mass transfer coefficient and a lower reaction energy consumption. Moreover, Co-CDs/AC demonstrated broad pH adaptability and long-term stability. The presence of CO_3^{2-} , $H_2PO_4^-$, or Cl^- inhibited HA degradation, whereas NO_3^- exhibited negligible effects. In addition, Co-CDs/AC electrode exhibited versatile applicability for degrading diverse organic contaminants in wastewater. Both $\bullet OH$ and H^* were involved in Co-CDs/AC system, while the H^* was the dominant reactive species responsible for HA removal. Differ from other advanced oxidation processes, electro-reduction replaced electro-oxidation as the dominant reaction in the degradation of HA. The Co-CDs/AC electrodes demonstrated significant potential for improving the biodegradability of HA-containing wastewater.

CRediT authorship contribution statement

Wenwen Zhang: Writing – review & editing, Writing – original draft, Methodology, Investigation, Formal analysis, Data curation. **Yufei Hui:** Writing – original draft, Visualization, Software, Investigation.

Jiahui Bi: Visualization, Software. **Hongjie Wang:** Writing – review & editing, Supervision, Methodology, Funding acquisition. **Wenyang Liang:** Writing – review & editing, Supervision, Methodology.

Declaration of competing interest

The authors declare that they have no known competing financial interests or personal relationships that could have appeared to influence the work reported in this paper.

Acknowledgments

This work was supported by the Core Talent Project under the Yanzhao Gold Terrace Attracting Talent Plan (Education Platform) of Hebei Province (HJZD202507), Natural Science Foundation of Hebei Province, China (B2025201010), and Collaborative Innovation Center for Baiyangdian Basin Ecological Protection and Beijing-Tianjin-Hebei Sustainable Development.

Appendix A. Supplementary data

Supplementary data to this article can be found online at <https://doi.org/10.1016/j.jenvman.2025.126768>.

Data availability

Data will be made available on request.

References

- Bazrafshan, E., Biglari, H., Mahvi, A.H., 2012. Humic acid removal from aqueous environments by electrocoagulation process using iron electrodes. *J. Chem.* 9, 2453–2461. <https://doi.org/10.1155/2012/876739>.
- Capasso, S., Salvestrini, S., Roviello, V., Trifuggi, M., Iovino, P., 2019. Electrochemical removal of humic acids from water using aluminum anode: influence of chloride ion and current parameters. *J. Chem.* 9, 5401475. <https://doi.org/10.1155/2019/5401475>.
- Chen, M., Ma, J., Feng, Y., Wu, Y., Hu, G., Liu, X.J.C.C.R., 2025. Advanced characterization enables a new era of efficient carbon dots electrocatalytic reduction. *Coord. Chem. Rev.* 535, 216612. <https://doi.org/10.1016/j.ccr.2025.216612>.
- Chen, W., Westerhoff, P., Leenheer, J.A., Booksh, K., 2003. Fluorescence excitation–emission matrix regional integration to quantify spectra for dissolved organic matter. *Environ. Sci. Technol.* 37, 5701–5710. <https://doi.org/10.1021/es0341354c>.
- Dargahi, A., Gilan, R.A., Samarghandi, M.R., ZolghadriNasab, H., Karimi, F., 2022. Electro-peroxymonosulfate processes for the removal of humic acid from aqueous media. *Biomass. Convers. Bior.* 14, 12731–12745. <https://doi.org/10.1007/s13399-022-03142-4>.
- Ding, M., Zhang, Q., Shi, F., Zhou, L., Guo, X., Li, Q., Luo, L., Miao, Y., Huo, Y., 2025. Initiative invasion promoted photoelectrocatalytic antibacterial function on ZIF-67@CoO/Co foil photoanode. *Chem. Eng. J.* 519, 165564. <https://doi.org/10.1016/j.cej.2025.165564>.
- Du, T., Zhang, G., Zou, J., 2022. Coupling photocatalytic and electrocatalytic oxidation towards simultaneous removal of humic acid and ammonia-nitrogen in landscape water. *Chemosphere* 286, 131717. <https://doi.org/10.1016/j.chemosphere.2021.131717>.
- Fan, T.-X., Cai, Y., Chu, G.-W., Luo, Y., Zhang, L.-L., Chen, J.-F., 2019. A novel rotating multielectrodes reactor for electrochemical oxidation process intensification. *Ind. Eng. Chem. Res.* 58, 2396–2404. <https://doi.org/10.1021/acs.iecr.8b05736>.
- Feng, Y., Lv, X., Wang, H., Wang, H., Yan, F., Wang, L., Wang, H., Ren, J.T., Yuan, Z.Y., 2025. H^* species regulation of heterostructured Co_2O_3/NiO nanoflowers boosting tandem nitrite reduction for high-efficiency ammonia production. *Adv. Funct. Mater.*, 2425687 <https://doi.org/10.1002/adfm.202425687>.
- Fukushima, M., Tatsumi, K., Nagao, S., 2001. Degradation characteristics of humic acid during photo-Fenton processes. *Environ. Sci. Technol.* 35, 3683–3690. <https://doi.org/10.1021/es0018825>.
- Gao, H.-Y., Huang, C.-H., Mao, L., Shao, B., Shao, J., Yan, Z.-Y., Tang, M., Zhu, B.-Z., 2020. First direct and unequivocal electron spin resonance spin-trapping evidence for pH-dependent production of hydroxyl radicals from sulfate radicals. *Environ. Sci. Technol.* 54, 14046–14056. <https://doi.org/10.1021/acs.est.0c04410>.
- Ge, H., Li, G., Shen, J., Ma, W., Meng, X., Xu, L., 2020. Co_4N nanoparticles encapsulated in N-doped carbon box as tri-functional catalyst for Zn-air battery and overall water splitting. *Appl. Catal. B Environ.* 275, 119104. <https://doi.org/10.1016/j.apcatb.2020.119104>.

- Gu, H., Xie, W., Du, A., Pan, D., Guo, Z., 2023. Overview of electrocatalytic treatment of antibiotic pollutants in wastewater. *Catal. Rev. Sci. Eng.* 65, 569–619. <https://doi.org/10.1080/01614940.2021.1960009>.
- Gudimella, K.K., Gedda, G., Kumar, P.S., Babu, B.K., Yamajala, B., Rao, B.V., Singh, P.P., Kumar, D., Sharma, A., 2022. Novel synthesis of fluorescent carbon dots from bio-based *Carica papaya* leaves: optical and structural properties with antioxidant and anti-inflammatory activities. *Environ. Res.* 204, 111854. <https://doi.org/10.1016/j.envres.2021.111854>.
- Guo, J., Lu, Y., Xie, A.Q., Li, G., Liang, Z.B., Wang, C.F., Yang, X., Chen, S.J.A.F.M., 2022. Yellow-emissive carbon dots with high solid-state photoluminescence. *Adv. Funct. Mater.* 32, 2110393. <https://doi.org/10.1002/adfm.202110393>.
- Hao, J.-N., Ding, Z.-Z., Shen, C.-L., Zheng, G.-S., Liu, J.-L., Li, R.-B., Song, R.-W., Liu, K.-K., Zang, J.-H., Dong, L., Lou, Q., Shan, C.-X., 2024. Ionic-confining-assisted multiple-mode tunable light emitting of carbon nanodots. *Chem. Eng. J.* 486, 150196. <https://doi.org/10.1016/j.cej.2024.150196>.
- He, S., Jiang, T., Ye, C., Wang, W., Tang, S., 2025. Spindle-shaped medium-entropy metal telluride nanostructures as high-performance dual-catalytic electrocatalysts for overall water splitting. *J. Colloid Interface Sci.* 695, 137749. <https://doi.org/10.1016/j.jcis.2025.137749>.
- Huang, X., Guo, Y., Zou, Y., Jiang, J., 2022. Electrochemical oxidation of glycerol to hydroxypruvic acid on cobalt (oxy)hydroxide by high-valent cobalt redox centers. *Appl. Catal. B Environ.* 309, 121247. <https://doi.org/10.1016/j.apcatb.2022.121247>.
- Huang, X., Wu, G., Song, Y., Wu, T., Sun, P., Zhu, X., Wang, J., Yin, X., Mo, Z., 2025. Enhancing photocatalytic hydrogen evolution of carbon nitride through high-valent cobalt active sites in cobalt sulfide co-catalyst. *J. Colloid Interface Sci.* 683, 546–554. <https://doi.org/10.1016/j.jcis.2024.12.198>.
- Jiang, J., Yang, M., Huang, M., Guo, X., Tao, X., Xu, L., Lu, Y., Tang, L., Cheng, Y., 2025. Transition metal-loaded granular activated carbon as efficient three-dimensional electrode for humic acid removal. *J. Environ. Sci.* <https://doi.org/10.1016/j.jes.2025.06.031>.
- Jiang, S., Cheng, S., Cao, J., Yue, C., Xiong, J., Jiang, C., Cai, H., Wu, J., 2024. Monodispersed Co-N₃ loaded carbon nitride mediated peroxymonosulfate activation for rapid degradation of trace urea via singlet oxygen. *Chem. Eng. J.* 479, 147526. <https://doi.org/10.1016/j.cej.2023.147526>.
- Jing, Q., Cai, J., Feng, K., Li, H., 2023. Remove humic acid from water quickly using only oxygen and sulfite at nickel cobalt spinel catalyst. *Environ. Res.* 220, 115209. <https://doi.org/10.1016/j.enres.2023.115209>.
- Lee, C.-S., Jeon, T.H., Jang, Y.H., Lim, H.J., Kwon, B.J., Kwon, O., Kumar, K., Sunariwal, N., Kim, T., 2024. Cobalt single-atom catalyst as a multifunctional electrocatalyst for boosting radical generation. *Chem. Eng. J.* 481, 148431. <https://doi.org/10.1016/j.cej.2023.148431>.
- Lei, Y., Lei, X., Westerhoff, P., Tong, X.Y., Ren, J.N., Zhou, Y.J., Cheng, S.S., Ouyang, G. F., Yang, X., 2022. Bromine radical (Br· and Br₂·) reactivity with dissolved organic matter and brominated organic byproduct formation. *Environ. Sci. Technol.* 56, 5189–5199. <https://doi.org/10.1021/acs.est.2c00549>.
- Lei, Y., Lei, X., Westerhoff, P., Zhang, X., Yang, X., 2021. Reactivity of chlorine radicals (Cl· and Cl₂·) with dissolved organic matter and the formation of chlorinated byproducts. *Environ. Sci. Technol.* 55, 689–699. <https://doi.org/10.1021/acs.est.0c05596>.
- Li, C., Luo, G., Liu, Y., 2023. Comparison of the ability of three advanced oxidation processes (AOPs) converting Cl⁻ to active inorganic chlorine species (AICS). *Process Saf. Environ. Prot.* 169, 959–969. <https://doi.org/10.1016/j.psep.2022.11.075>.
- Li, J., Wang, L., Lu, J.B., Peng, W.L., Chen, J., Jiang, G.M., Liu, D.F., 2024b. Treatment of landfill leachate nanofiltration concentrate by a three-dimensional electrochemical technology with waste aluminum scraps as particle electrodes: efficacy, mechanisms, and enhancement effect of subsequent electrocoagulation. *Waste Manag.* 173, 118–130. <https://doi.org/10.1016/j.wasman.2023.11.016>.
- Li, W., Xiao, M., Jiang, J., Li, Y., Zhang, X., Li, S., Lin, X., Peng, D., Or, S.W., Sun, S., Xing, Z., 2025. Co₄N nanoparticles embedded in N-doped carbon pores: advanced interlayer material for lithium-sulfur batteries. *Nano Energy* 142, 111140. <https://doi.org/10.1016/j.nanoen.2025.111140>.
- Li, X., Fu, Y., Zhao, S., Xiao, J., Lan, M., Wang, B., Zhang, K., Song, X., Zeng, L., 2022. Metal ions-doped carbon dots: synthesis, properties, and applications. *Chem. Eng. J.* 430, 133101. <https://doi.org/10.1016/j.cej.2021.133101>.
- Li, G., Liu, W., Gao, S., Lu, H., Fu, D., Wang, M., Liu, X., 2024a. MXene-based composite aerogels with bifunctional ferrous ions for the efficient degradation of phenol from wastewater. *Chemosphere* 358, 142151. <https://doi.org/10.1016/j.chemosphere.2024.142151>.
- Li, X., Lu, S., Zhang, G., 2023. Three-dimensional structured electrode for electrocatalytic organic wastewater purification: design, mechanism and role. *J. Hazard. Mater.* 445, 130524. <https://doi.org/10.1016/j.jhazmat.2022.130524>.
- Li, Z., Kang, W., Lin, J., Li, R., Qu, K., Zeng, S., Wang, L., Meng, F., Zhang, H., Li, H., 2025. Single-atom Co meets remote Fe for a synergistic boost in oxygen electrocatalysis. *Adv. Energy Mater.*, 2500617 <https://doi.org/10.1002/aenm.202500617>.
- Liang, F., Wei, X., Zhou, X., Guo, Y., Miao, J., Xu, H., Lu, W., Zhang, R., Zhang, N., Peng, S., 2024. Nitrogen-doped carbon aerogel supported SnO₂ anode for electrocatalytic degradation of phenol: enhanced generation of free radicals. *Colloid. Surf. A-Physicochem. Eng. Asp.* 688, 133636. <https://doi.org/10.1016/j.colsurfa.2024.133636>.
- Liu, H.Y., Jin, Q.H., Wu, X.X., 2024. Intramolecular hydrogen atom transfer from unactivated C(sp³)–H bond to alkyl radical. *Eur. J. Org. Chem.* 27, e202301280. <https://doi.org/10.1002/ejoc.202301280>.
- Liu, Z., Meng, H., Li, C., Liu, T., Cao, J., Lv, Y., 2019a. Catalytic degradation of humic acid by Mn-Cu/Al-MCM-41 catalyst in electro-fenton/Chlorine processes: influencing factors, mechanisms, and kinetics. *Water. Air. Soil. Pollut.* 230, 230. <https://doi.org/10.1007/s11270-019-4288-5>.
- Liu, H., Han, J., Yuan, J., Liu, C., Wang, D., Liu, T., Liu, M., Luo, J., Wang, A., Crittenden, J.C., 2019b. Deep dehalogenation of florfenicol using crystalline Co⁹ nanosheet arrays on a Ti plate via direct cathodic reduction and atomic H. *Environ. Sci. Technol.* 53, 11932–11940. <https://doi.org/10.1021/acs.est.9b04352>.
- Lizhang, W., Shengxiang, Y., Bo, W., Peng, L., Zhe'nan, L., Yuemin, Z., 2016. The influence of anode materials on the kinetics toward electrochemical oxidation of phenol. *Electrochim. Acta* 206, 270–277. <https://doi.org/10.1016/j.electacta.2016.04.168>.
- Lu, Y., Bian, Z., Chu, F., Lu, J., Hou, G., Hou, S., 2023. Study on the tunable fluorescence emission mechanism of nitrogen-doped carbon dots and ion sensing potential applications. *J. Electron. Mater.* 52, 5946–5954. <https://doi.org/10.1007/s11664-023-10426-6>.
- Lyman, S.V., Schwarz, H.A., 2012. Hydrogen atom reactivity toward aqueous tert-butyl alcohol. *J. Phys. Chem. A* 116, 1383–1389. <https://doi.org/10.1021/jp2116593>.
- Lyu, J., Zhang, T., Li, J., 2025. Comparative study on Co³⁺, Co²⁺, and oxygen vacancies in the photocatalytic ozonation of VOCs on Co₃O₄ crystal facets. *Sep. Purif. Technol.* 363, 132072. <https://doi.org/10.1016/j.seppur.2025.132072>.
- Mezky, S.P., Cooper, W.J., Madden, K.P., Bartels, D.M., 2004. Free radical destruction of N-nitrosodimethylamine in water. *Environ. Sci. Technol.* 38, 3161–3167. <https://doi.org/10.1021/es0347742>.
- Mielnik, L., Kowalczyk, P., 2018. Optical characteristic of humic acids from Lake sediments by excitation-emission matrix fluorescence with PARAFAC model. *J. Soils Sediments* 18, 2851–2862. <https://doi.org/10.1007/s11368-018-1947-x>.
- Mohsin, M., Bhatti, I.A., Ashar, A., Khan, M.W., Farooq, M.U., Khan, H., Hussain, M.T., Loomba, S., Mohiuddin, M., Zavabeti, A., Ahmad, M., Yousaf, M., Mahmood, N., 2021. Iron-doped zinc oxide for photocatalyzed degradation of humic acid from municipal wastewater. *Appl. Mater. Today* 23, 101047. <https://doi.org/10.1016/j.apmt.2021.101047>.
- Qin, H., Wang, Y., Wang, B., Duan, X., Lei, H., Zhang, X., Zheng, H., Zhang, W., Cao, R., 2021. Cobalt porphyrins supported on carbon nanotubes as model catalysts of metal-N₄/C sites for oxygen electrocatalysis. *J. Energy Chem.* 53, 77–81. <https://doi.org/10.1016/j.jechem.2020.05.015>.
- Rani, U.A., Ng, L.Y., Ng, C.Y., Mahmoudi, E., 2020. A review of carbon quantum dots and their applications in wastewater treatment. *Adv. Colloid Interface Sci.* 278, 102124. <https://doi.org/10.1016/j.cis.2020.102124>.
- Sarno, M., Scuderi, C., Ponticorvo, E., 2019. A new nanohybrid for electrochemical removal of humic acids and Cr(VI). *Water. Environ. Justice* 34, 131–138. <https://doi.org/10.1111/wej.12512>.
- Satishkumar, P., Isloor, A.M., Farnood, R., 2025. High performance 2D molybdenum MXene polyphenylsulfone membranes for boosting water flux and efficient removal of humic acid, antibiotic and dyes from wastewater. *Chem. Eng. J.* 512, 161920. <https://doi.org/10.1016/j.cej.2025.161920>.
- Sierra, M.M., Giovanelia, M., Parlanti, E., Soriano-Sierra, E.J., 2005. Fluorescence fingerprint of fulvic and humic acids from varied origins as viewed by single-scan and excitation/emission matrix techniques. *Chemosphere* 58, 715–733. <https://doi.org/10.1016/j.chemosphere.2004.09.038>.
- Tang, C., Yan, W., Zheng, C., 2014. Electrochemical oxidation of humic acid at the antimony- and nickel-doped tin oxide electrode. *Front. Environ. Sci. Eng.* 8, 337–344. <https://doi.org/10.1007/s11783-013-0545-9>.
- Trelli, C., Pechaud, Y., Oturan, N., Mousset, E., Huguenot, D., van Hullebusch, E., Esposito, G., Oturan, M., 2016. Comparative study on the removal of humic acids from drinking water by anodic oxidation and electro-Fenton processes: mineralization efficiency and modelling. *Appl. Catal. B Environ.* 194. <https://doi.org/10.1016/j.apcatb.2016.04.039>.
- Valencia, S., Marín, J.M., Restrepo, G., Frimmel, F.H., 2013. Application of excitation–emission fluorescence matrices and UV/Vis absorption to monitoring the photocatalytic degradation of commercial humic acid. *Sci. Total Environ.* 442, 207–214. <https://doi.org/10.1016/j.scitotenv.2012.10.058>.
- Veerasubramani, G.K., Krishnamoorthy, K., Radhakrishnan, S., Kim, N.-J., Kim, S.J., 2014. Synthesis, characterization, and electrochemical properties of CoMoO₄ nanostructures. *Int. J. Hydrogen Energy* 39, 5186–5193. <https://doi.org/10.1016/j.ijhydene.2014.01.069>.
- Wang, J., Li, T., Zhou, M., Li, X., Yu, J., 2015. Characterization of hydrodynamics and mass transfer in two types of tubular electrochemical reactors. *Electrochim. Acta* 173, 698–704. <https://doi.org/10.1016/j.electacta.2015.05.135>.
- Wang, J., Wang, S., 2021. Effect of inorganic anions on the performance of advanced oxidation processes for degradation of organic contaminants. *Chem. Eng. J.* 411, 128392. <https://doi.org/10.1016/j.cej.2020.128392>.
- Wang, K., Zhao, K., Qin, X., Chen, S., Yu, H., Quan, X., 2022. Treatment of organic wastewater by a synergic electrocatalysis process with Ti³⁺ self-doped TiO₂ nanotube arrays electrode as both cathode and anode. *J. Hazard. Mater.* 424, 127747. <https://doi.org/10.1016/j.jhazmat.2021.127747>.
- Wang, L., Wang, B., Lu, S., Lv, S., Qu, X., 2025. High quantum yield yellow emission carbon dots for the construction of blue light blocking films. *Chin. Chem. Lett.* 36, 110497. <https://doi.org/10.1016/j.cclet.2024.110497>.
- Wang, X.-Y., Jiao, K.-N., Ying, L., Huang, Y.-F., Wang, Z.-F., 2025. Mixed-valence Ce–Fe bimetallic MOFs with multi-enzyme-like activities for colorimetric biosensing and catalytic degradation. *J. Colloid Interface Sci.*, 137784 <https://doi.org/10.1016/j.jcis.2025.137784>.
- Wang, X., Feng, Y., Dong, P., Huang, J., 2019. A mini review on carbon quantum dots: preparation, properties, and electrocatalytic application. *Front. Chem.* 7, 671. <https://doi.org/10.3389/fchem.2019.00671>.
- Wang, Y., Li, H., Zhou, W., Zhang, X., Zhang, B., Yu, Y., 2022. Structurally disordered RuO₂ nanosheets with rich oxygen vacancies for enhanced nitrate electroreduction

- to ammonia. *Angew Chem. Int. Ed. Engl.* 61, e202202604. <https://doi.org/10.1002/anie.202202604>.
- Wen, Y., Chen, J., Gao, X., Liu, W., Che, H., Liu, B., Ao, Y., 2023. Two birds with one stone: Cobalt-doping induces to enhanced piezoelectric property and persulfate activation ability of ZnO nanorods for efficient water purification. *Nano Energy* 107, 108173. <https://doi.org/10.1016/j.nanoen.2023.108173>.
- Wu, G., Wang, F., Yang, J., Hu, Z., Li, S., Huang, J., 2024. Preparation of MoSe₂ nanosheets/nitrogen-doped carbon nanotubes and their electrochemical energy storage properties. *Appl. Surf. Sci.* 678, 161087. <https://doi.org/10.1016/j.apsusc.2024.161087>.
- Wu, K., Cao, J., Zhang, R., Pei, Y., Peng, T., Chen, G., 2025. Micro-doping tin-bismuth on modification of Co₃O₄ electrocatalyst and degradation of ammonia nitrogen. *Environ. Res.* 275, 121366. <https://doi.org/10.1016/j.envres.2025.121366>.
- Xu, D., Li, Y., Yin, L., Ji, Y., Niu, J., Yu, Y., 2018. Electrochemical removal of nitrate in industrial wastewater. *Front. Environ. Sci. Eng.* 12, 9. <https://doi.org/10.1007/s11783-018-1033-z>.
- Xu, X., Qin, J., Wei, Y., Ye, S., Shen, J., Yao, Y., Ding, B., Shu, Y., He, G., Chen, H., 2019. Heterogeneous activation of persulfate by NiFe_{2-x}Co_xO₄-RGO for oxidative degradation of bisphenol A in water. *Chem. Eng. J.* 365, 259–269. <https://doi.org/10.1016/j.cej.2019.02.019>.
- Xu, X., Zeng, X., Zhang, C., Huang, R., Ding, W., 2023. Enhanced electrocatalytic removal of tetracycline using dual carbon material combined particle electrodes in a three-dimensional electrochemical system: degradation pathway and mechanism. *J. Clean. Prod.* 419, 138257. <https://doi.org/10.1016/j.jclepro.2023.138257>.
- Yang, M., Feng, T., Chen, Y., Zhao, X., Yang, B., 2019. Ionic-state cobalt and iron Co-doped carbon dots with superior electrocatalytic activity for the oxygen evolution reaction. *Chemelectrochem* 6, 2088–2094. <https://doi.org/10.1002/celc.201900423>.
- Yang, Y., Ma, N., Wang, H., Liang, Q., Bian, Z., 2019. Pd-Ag/graphene electrochemical sensor for chlorophenol contaminant determination. *J. Electrochem. Soc.* 166, B266–B275. <https://doi.org/10.1149/2.1011904jes>.
- Yang, Y., Zeng, R., Xiong, Y., DiSalvo, F.J., Abruna, H.D., 2019. Cobalt-based nitride-core oxide-shell oxygen reduction electrocatalysts. *J. Am. Chem. Soc.* 141, 19241–19245. <https://doi.org/10.1021/jacs.9b10809>.
- Ye, X.C., Yao, J., Dong, Z.K., Zhang, Y., 2023. Enhanced electroactivation of peroxydisulfate with Fe-doped MoS₂ and GAC particle electrodes as heterogenous catalyst for the degradation of carbamazepine. *J. Environ. Eng.* 149, 04023052. <https://doi.org/10.1061/joeedu.Eeeng-7361>.
- Yin, H., Guo, Q., Lei, C., Chen, W., Huang, B., 2020. Electrochemical-driven carbocatalysis as highly efficient advanced oxidation processes for simultaneous removal of humic acid and Cr(VI). *Chem. Eng. J.* 396, 125156. <https://doi.org/10.1016/j.cej.2020.125156>.
- Yu, J., Zou, J., Xu, P., He, Q., 2020. Three-dimensional photoelectrocatalytic degradation of the opaque dye acid fuchsin by Pr and Co co-doped TiO₂ particle electrodes. *J. Clean. Prod.* 251, 119744. <https://doi.org/10.1016/j.jclepro.2019.119744>.
- Zhang, C., Huang, N., Zhai, Z., Liu, L., Chen, B., Yang, B., Jiang, X., Yang, N.J.A.E.M., 2023. Bifunctional oxygen electrocatalyst of Co₃N and nitrogen-doped carbon nanowalls/diamond for high-performance flexible Zinc-Air batteries. *Adv. Energy Mater.* 13, 2301749. <https://doi.org/10.1002/aenm.202301749>.
- Zhang, J., Li, C., Zhang, M., Zhang, J., Wu, X., Li, X., Lü, W., 2020. Cobalt and nitrogen codoped carbon nanotubes derived from a graphitic C₃N₄ template as an electrocatalyst for the oxygen reduction reaction electronic supplementary information (ESI) available. *Nanoscale. Adv.* 2, 3963–3971. <https://doi.org/10.1039/d0na00502a>.
- Zhang, J., Qu, S., 2024. Synergetic multiple free radicals lower the organohalide conversion barrier and potentiate effective contaminant mineralization. *Appl. Catal. B Environ.* 343, 123554. <https://doi.org/10.1016/j.apcatb.2023.123554>.
- Zhang, Q., Peng, Q.Y., Li, W.B., Liu, Y.Z., Wang, X.X., 2023. Waste plastic recycling upgrade design nanogenerator for catalytic degradation of pollutants. *Catalysts* 13, 1019. <https://doi.org/10.3390/catal13061019>.
- Zhang, W., Xie, D., Li, X., Ye, W., Jiang, X., Wang, Y., Liang, W., 2018. Electrocatalytic removal of humic acid using cobalt-modified particle electrodes. *Appl. Catal. A-Gen.* 559, 75–84. <https://doi.org/10.1016/j.apcata.2018.04.012>.
- Zhang, W., Ye, W., Hu, X., Liang, W., 2021. Electrocatalytic degradation of humic acid using particle electrodes of activated carbon loaded with metallic cobalt. *Chemosphere* 263, 128200. <https://doi.org/10.1016/j.chemosphere.2020.128200>.
- Zhang, Z., Yi, G., Li, P., Wang, X., Wang, X., Zhang, C., Zhang, Y., 2021. Recent progress in engineering approach towards the design of PbO₂-based electrodes for the anodic oxidation of organic pollutants. *J. Water Process Eng.* 42, 102173. <https://doi.org/10.1016/j.jwpe.2021.102173>.
- Zhao, G., Tao, X., Guo, T., Fu, L., Yang, H.J.A.N., 2024. Mineral-mediated epitaxial growth of CoO nanoparticles for efficient electrochemical H₂O₂ activation. *ACS Nano* 19, 1509–1518. <https://doi.org/10.1021/acsnano.4c14453>.
- Zhou, M., Zhou, Z., Gong, A., Zhang, Y., Li, Q., 2015. Synthesis of highly photoluminescent carbon dots via citric acid and Tris for iron(III) ions sensors and bioimaging. *Talanta* 143, 107–113. <https://doi.org/10.1016/j.talanta.2015.04.015>.
- Zhou, M.H., Dai, Q.Z., Lei, L.C., Wu, Z.C., Ma, C.A., Wang, D.H., 2004a. Electrochemical oxidation for the degradation of organic pollutants on a novel PbO₂ anode. *Acta Phys. - Chim. Sin.* 20, 871–876. <https://doi.org/10.3866/pku.Wlxh20040818>.
- Zhou, M.H., Wu, Z.C., Ma, X.J., Cong, Y.Q., Ye, Q., Wang, D.H., 2004b. A novel fluidized electrochemical reactor for organic pollutant abatement. *Sep. Purif. Technol.* 34, 81–88. [https://doi.org/10.1016/s1383-5866\(03\)00178-3](https://doi.org/10.1016/s1383-5866(03)00178-3).
- Zhu, X., Liu, J., Li, L., Zhen, G., Lu, X., Zhang, J., Liu, H., Zhou, Z., Wu, Z., Zhang, X., 2023. Prospects for humic acids treatment and recovery in wastewater: a review. *Chemosphere* 312, 137193. <https://doi.org/10.1016/j.chemosphere.2022.137193>.
- Zu, F., Yan, F., Bai, Z., Xu, J., Wang, Y., Huang, Y., Zhou, X., 2017. The quenching of the fluorescence of carbon dots: a review on mechanisms and applications. *Microchim. Acta* 184, 1899–1914. <https://doi.org/10.1007/s00604-017-2318-9>.